PNAS RESEARCH ARTICLE | MICROBIOLOGY

FeMV is a cathepsin-dependent unique morbillivirus infecting the kidneys of domestic cats

Sham Nambulli[a,b,c,1], Linda J. Rennick[a,b,c,1], Andrew S. Acciardo[c], Natasha L. Tilston-Lunel[a,b,c], Gregory Ho[c], Nicholas A. Crossland[c,d], Kathy Hardcastle[c], Betsy Nieto[e], Graeme Bainbridge[e], Tracey Williams[e], Claire R. Sharp[f,g], and W. Paul Duprex[a,b,c,2]

Edited by Diane Griffin, Johns Hopkins University, Baltimore, MD; received June 1, 2022; accepted August 11, 2022

Feline morbillivirus (FeMV) is a recently discovered pathogen of domestic cats and has been classified as a morbillivirus in the *Paramyxovirus* family. We determined the complete sequence of FeMV^{US5} directly from an FeMV-positive urine sample without virus isolation or cell passage. Sequence analysis of the viral genome revealed potential divergence from characteristics of archetypal morbilliviruses. First, the virus lacks the canonical polybasic furin cleavage signal in the fusion (F) glycoprotein. Second, conserved amino acids in the hemagglutinin (H) glycoprotein used by all other morbilliviruses for binding and/or fusion activation with the cellular receptor CD150 (signaling lymphocyte activation molecule [SLAM]/F1) are absent. We show that, despite this sequence divergence, FeMV H glycoprotein uses feline CD150 as a receptor and cannot use human CD150. We demonstrate that the protease responsible for cleaving the FeMV F glycoprotein is a cathepsin, making FeMV a unique morbillivirus and more similar to the closely related zoonotic Nipah and Hendra viruses. We developed a reverse genetics system for FeMV^{US5} and generated recombinant viruses expressing Venus fluorescent protein from an additional transcription unit located either between the phosphoprotein (*P*) and matrix (*M*) genes or the *H* and large (*L*) genes of the genome. We used these recombinant FeMVs to establish a natural infection and demonstrate that FeMV causes an acute morbillivirus-like disease in the cat. Virus was shed in the urine and detectable in the kidneys at later time points. This opens the door for long-term studies to address the postulated role of this morbillivirus in the development of chronic kidney disease.

morbillivirus | chronic kidney disease | feline | cathepsin | pathogenesis

Significance

Feline morbillivirus (FeMV) has been classified as a morbillivirus despite lacking several biological features shared by all other known viruses in the genus. We confirm that FeMV uses CD150 as a cellular receptor and employs a different protease to furin to process the fusion glycoprotein. As such, FeMV may represent an important evolutionary intermediate between morbilliviruses and the zoonotic henipaviruses. Feline chronic kidney disease is the leading cause of morbidity and mortality in cats and has no clear etiology. FeMV has been postulated to be a causative agent. We dissected FeMV pathogenesis using recombinant, fluorescent protein expressing viruses based on an unpassaged clinical isolate. This sheds light on the primary target cells infected and possible mechanisms of host-to-host transmission.

Feline morbillivirus (FeMV) is a negative-sense, single-stranded, nonsegmented RNA virus with a genome composed of 16,050 nucleotides first discovered in domestic cats in Hong Kong and China in 2012 (1). Sequence analysis of the complete genome suggested that FeMV was a member of the *Morbillivirus* genus within the *Paramyxovirus* family. It has six transcription units, corresponding to 3′ N-P/V/C-M-F-H-L 5′ of the other morbilliviruses, including a phospho- protein (*P*) gene that contains an overlapping reading frame corresponding to the nonstructural C protein and an editing site that would allow generation of a V protein (1). The genome conforms to the "rule of six," a requirement for efficient replication of all morbillivirus and some paramyxovirus genomes (2), although adherence has not been proven experimentally for FeMV. The 3′ noncoding terminus of FeMV is 107 nucleotides long, which is identical to those of the other morbilliviruses, and the $(CN_5)_3$ motif, shown to be necessary for morbillivirus genome replication, is conserved at nucleotide positions 79, 85, and 91 (3).

Another defining characteristic of all morbilliviruses is their use of signaling lymphocyte activation molecule/F1 (or CD150) as the primary entry receptor. This has been debated to be a criterion to classify a virus as a morbillivirus (3, 4). Sequence analysis of FeMV hemagglutinin (H) glycoprotein (5) suggests that it lacks the conserved residues required for the measles virus (MV) H glycoprotein/CD150 interaction (6), amino acids also conserved in other morbillivirus H glycoproteins (*SI Appendix*, Table S1). This raises the question of whether FeMV is actually a "true" morbillivirus (3). Similarly, all previously identified morbilliviruses contain a polybasic furin cleavage signal in their fusion (F) glycoprotein. This facilitates cleavage of the F_0 precursor protein, by furin, into disulfide-linked F_1 and F_2 subunits, an essential process in the paramyxovirus life cycle (7). FeMV lacks a polybasic cleavage signal at the predicted cleavage site in the F glycoprotein, having only a single basic residue at this position (1), suggesting that it may utilize a fundamentally different activation strategy to all other morbilliviruses.

Since its discovery, FeMV has been postulated to play a role in the development of feline chronic kidney disease (CKD). In the original report (1), necropsy tissues of two FeMV-positive cats were analyzed and revealed kidney damage consistent with

Author contributions: S.N., L.J.R., K.H., B.N., G.B., T.W., C.R.S., and W.P.D. designed research; S.N., L.J.R., A.S.A., N.L.T.-L., G.H., N.A.C., K.H., and W.P.D. performed research; S.N., L.J.R., A.S.A., N.L.T.-L., G.H., N.A.C., K.H., C.R.S., and W.P.D. analyzed data; and S.N., L.J.R., and W.P.D. wrote the paper.

The authors declare no competing interest.

This article is a PNAS Direct Submission.

[1]S.N. and L.J.R. contributed equally to this work.

[2]To whom correspondence may be addressed. Email: pduprex@pitt.edu.

This article contains supporting information online at http://www.pnas.org/lookup/suppl/doi:10.1073/pnas.2209405119/-/DCSupplemental.

Published October 17, 2022.

tubulointerstitial nephritis (TIN). A follow-up case control study then showed TIN in 7 of 12 FeMV-positive cats but in only 2 of 15 FeMV-negative cats, suggesting an association between the FeMV infection and the TIN diagnosis (1). FeMV was subsequently reported elsewhere in Asia (8–13) and in Europe (14–16), North America (17), and South America (18, 19) with varied conclusions as to whether FeMV was potentially associated with CKD (10, 15, 16, 20) or not (8, 13, 14, 18, 21).

We previously demonstrated the existence of FeMV in the United States (17), reporting the complete genome sequence of FeMV^{US1}, a strain that is 98% identical to the previously published Asian FeMV^{776U} sequence (1) within the *H* gene. Importantly, we demonstrated detection of FeMV RNA from a clinically healthy cat in longitudinal urine samples collected over 15 months, proving that cats can be chronically infected with FeMV. Animals persistently shed the virus in their urine, a characteristic that may be important for a pathogen involved in the etiology of CKD, which progresses over many years, and in host-to-host transmission. In that publication, we also reported the *H* gene sequence of FeMV^{US5}, a strain that is only 86% identical to FeMV^{776U}. In this study, we obtain a complete genome sequence of this unpassaged clinical isolate of FeMV^{US5} and generate a reverse genetics system based on it. We examine CD150 receptor usage and demonstrate FeMV adherence to the "rule of six". We determined the protease necessary for F_0 cleavage both by transient transfection studies using cloned glycoproteins and in the context of recombinant feline morbillivirus (rFeMV). Finally, we developed a feline model of FeMV infection and demonstrate that FeMV causes a lymphotropic morbillivirus-like disease in the natural host when animals are infected by the respiratory route. This model will be indispensable in studies to determine if chronic FeMV infection plays the postulated role in the development of feline CKD and for transmission studies.

Results

FeMV Uses Feline CD150 as a Cellular Receptor. A quantitative dual bimolecular complementation assay (Fig. 1*A*) was used to examine receptor usage by the F and H glycoproteins of three different FeMV strains (US1, US2, and US5).

As anticipated, when two populations of Crandell–Rees feline kidney (CRFK) cells were transfected, no signal was generated (Fig. 1*B* and *SI Appendix*, Fig. S1, *Top*). Controls with MV and canine distemper virus (CDV) glycoproteins substituted for the FeMV glycoproteins also failed to produce a signal; substitution with the F and G glycoproteins from Nipah virus (NiV) that uses ephrin B2 as a receptor (22, 23), a molecule we thought likely to be present on CRFK cells, acted as a positive control. In contrast, when CRFK-feCD150 cells were used in the assay, a signal was generated for all of the FeMV strains (Fig. 1*B* and *SI Appendix*, Fig. S1, *Middle*), and MV and CDV glycoprotein expression also led to signal generation, indicating that these morbillivirus glycoproteins can also use feline CD150 (feCD150) as a receptor. When human CD150 (hCD150) was substituted for feCD150, only MV glycoprotein expression led to signal generation (Fig. 1*B* and *SI Appendix*, Fig. S1, *Bottom*), indicating that FeMV cannot use hCD150 as was already known for CDV (24).

FeMV Glycoprotein-Induced Fusion Is Dependent on Cysteine Protease Availability. Alignment of the amino acid sequence of the F glycoprotein of FeMV^{US5} with those of MV^{KS} and

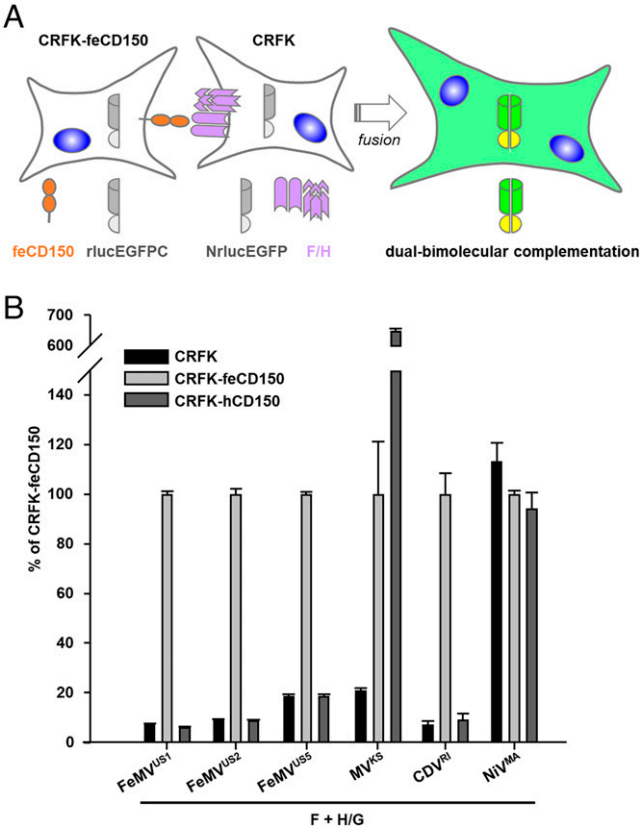

Fig. 1. FeMV glycoproteins can use feCD150. (*A*) Summary of the dual bimolecular complementation assay. CRFK-feCD150 (or CFRK-hCD150 or CRFK for controls) and CRFK cell populations are transfected with pCG-rlucEGFPC and pCG-NrlucEGFP, respectively. CRFK cells are simultaneously transfected with FeMV, MV, or canine distemper virus (CDV) F and H glycoproteins (or F/G for Nipah [NiV]). After 24 h, the cell populations are trypsinized and mixed. Glycoprotein-induced fusion of the cell populations results in *Renilla* luciferase (rLuc)-enhanced green fluorescent protein (EGFP) complementation, leading to EGFP fluorescence and *Renilla* luciferase activity. (*B*) Relative luminescence detected when CRFK cells expressing various viral F and H/G glycoprotein pairs and NrlucEGFP are mixed with CRFK cells, CRFK-feCD150, or CRFK-hCD150 cells expressing rlucEGFPC and triplicate cell monolayers are lysed and assayed for luciferase activity. Luminescence produced when CRFK cells expressing the glycoprotein pairs are mixed with CRFK-feCD150 cells is set to 100%.

CDV^{RI} reveals only a single basic residue (Arg/R) at the putative cleavage site (Fig. 2*A*).

The closely related paramyxoviruses NiV and Hendra virus (refs. 1 and 3 have phylogenetic trees) also contain monobasic cleavage signals in their F glycoproteins and have been shown to use the cysteine proteases, cathepsins, for their cleavage (25–27). Lysates from CRFK-feCD150 cells transfected with a vector expressing AU1-tagged FeMV^{US5}F in the absence or presence of the pancysteine protease inhibitor E64d were prepared and analyzed (Fig. 2*B*). Unprocessed F_0 and the F_1 subunit could be detected in cells treated with dimethyl sulfoxide (DMSO) as a control (lane 2 in Fig. 2*B*), indicating that FeMV^{US5}F was processed as predicted from the sequence alignment (Fig. 2*A*). F_0 was detected in cells treated with E64d (lane 3 in Fig. 2*B*), but the postprocessing F_1 subunit was not, indicating that E64d prevented FeMV^{US5}F processing and showing that a cysteine protease was responsible.

We generated FeMV$^{US5}F_{PB}$ by inserting a polybasic cleavage signal into the FeMV^{US5}F glycoprotein (Fig. 2*A*) based on the CDV^{RI}F sequence (accession no. AMH87497.1) since this had the most sequence similarity to FeMV^{US5}F in that region. Lysates from CRFK-feCD150 cells transfected with a vector

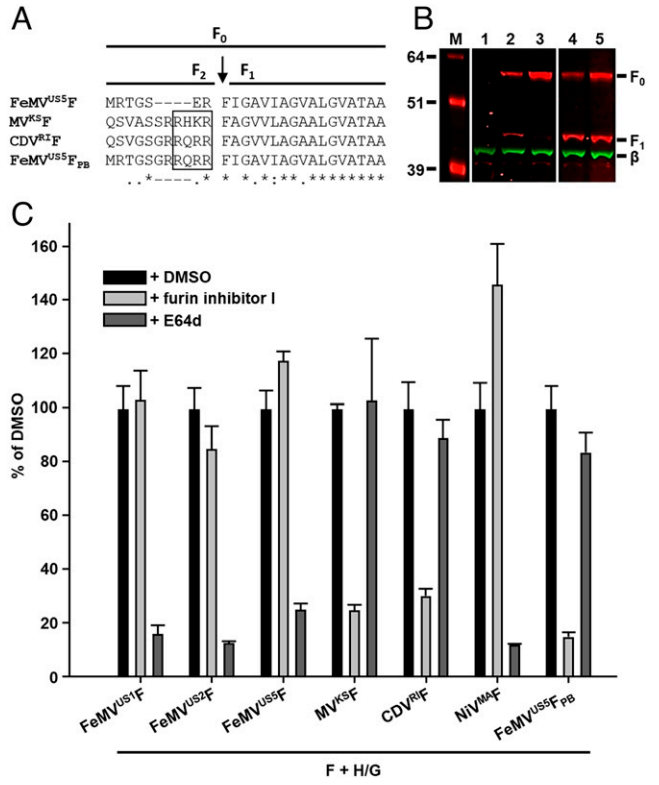

Fig. 2. FeMV glycoprotein-induced cell-to-cell fusion is inhibited by a cysteine protease inhibitor. (*A*) Alignment of the predicted cleavage site and surrounding sequences of the FeMV^{US5} F glycoprotein with the equivalent regions of MV^{KS} and CDV^{RI} F glycoproteins and a modified FeMV^{US5} F glycoprotein engineered to contain a polybasic cleavage signal (FeMV^{US5}F$_{PB}$). The polybasic cleavage signal is boxed, and an arrow marks the predicted cleavage site in F_0, which gives rise to F_1 and F_2 subunits, (-) amino acid absent in sequence aligment, (*) conserved amino acid in sequence aligment, (.) conservative replacement of amino acid in sequence alignment. (*B*) Western blot analysis of transfected CRFK-feCD150 cell lysates. Cells were transfected with pCG-FeMV^{US5}F (lane 1) as a background blotting control or with pCG-FeMV^{US5}F$_{AU1}$ (lanes 2 and 3) or pCG-FeMV^{US5}F$_{PB\text{-}AU1}$ (lanes 4 and 5). Transfected cells were treated with DMSO (lanes 1, 2, and 4) or E64d cysteine protease inhibitor (lanes 3 and 5). F glycoproteins were detected with anti-AU1 antibody (red), and an anti−β-actin antibody was used as a loading control (β; 42 kDa; green). The predicted F_0 (61-kDa) and F_1 (49-kDa) subunits are indicated based on the marker sizes (lane M). (*C*) Relative luminescence detected when CRFK cells expressing various viral F and H (or F/G for NiV) glycoprotein pairs and NrlucEGFP are mixed with CRFK-feCD150 cells expressing rlucEGFPC in the presence of DMSO, furin inhibitor I, or E64d cysteine protease inhibitor and triplicate cell monolayers are lysed and assayed for luciferase activity. Luminescence produced when fusion assays were carried out in the presence of DMSO is set to 100%.

expressing AU1-tagged FeMV^{US5}F$_{PB}$ in the absence or presence of E64d were prepared and analyzed (Fig. 2*B*). In cells treated with DMSO (lane 4 in Fig. 2*B*), F_0 and the F_1 subunit could be detected. In cells treated with E64d (lane 5 in Fig. 2*B*), both F_0 and F_1 subunit could still be detected, indicating that E64d no longer prevented F_0 glycoprotein processing and that a cysteine protease was no longer responsible for FeMV^{US5}F$_{PB}$ processing.

We investigated this further by performing the bimolecular complementation assay in the presence of E64d cysteine protease inhibitor or furin inhibitor I. In the presence of DMSO (Fig. 2*C* and *SI Appendix*, Fig. S2, *Top*), all viral glycoproteins induced expected levels of fusion. In the presence of furin inhibitor I (Fig. 2*C* and *SI Appendix*, Fig. S2, *Middle*), FeMV glycoprotein-induced fusion was unaffected, while the control MV^{KS} and CDV^{RI} glycoprotein-induced fusion (furin dependent) was reduced. In the presence of E64d (Fig. 2*C* and *SI Appendix*, Fig. S2, *Bottom*), FeMV glycoprotein-induced fusion was significantly reduced, as was control NiV^{MA} glycoprotein-induced fusion (cathepsin dependent). As anticipated, in assays using the FeMV^{US5}F$_{PB}$ protein, E64d treatment (Fig. 2*C* and *SI Appendix*, Fig. S2, *Bottom*) no longer affected the fusion activity, while furin inhibitor I treatment (Fig. 2*C* and *SI Appendix*, Fig. S2, *Middle*) significantly reduced fusion, indicating that we had been successful in switching the protease dependence of the protein.

Generation of an FeMV Reverse Genetics System. We determined the full genomic sequence of FeMV^{US5} using primers (*SI Appendix*, Table S2) to generate complementary (c) DNA from clinical material and obtain PCR amplicons, which were purified and consensus sequenced. Importantly, this entire sequence was derived directly from a clinical sample and not from a virus that had been isolated and grown in cell culture. Large amplicons from the FeMV^{US5} sequence determination were subcloned, a cloning strategy was devised, and a full-length genomic pFeMV^{US5} clone was assembled sequentially. This molecular clone was modified to include an additional transcription unit (ATU) encoding Venus fluorescent protein between the *H* and large (*L*) genes to generate pFeMV^{US5}Venus(6) or between the *P* and matrix (*M*) genes to generate pFeMV^{US5}Venus(3) (Fig. 3*A*).

Viruses were recovered using CRFK-feCD150 cells to ensure the virus did not evolve to use an unnatural entry pathway or accumulate spurious mutations. The Venus protein allowed infected cells to be identified by fluorescence microscopy even when the cytopathic effect is not readily identifiable by phase microscopy (*SI Appendix*, Fig. S3). This was vitally important given the cell-associated growth properties of FeMV. Virus stocks were generated, and the growth kinetics in CRFK-feCD150 cells were determined (Fig. 3*B*). Both viruses grew similarly for the first 4 d postinfection (d.p.i.).

FeMV Obeys the "Rule of Six". The FeMV^{US5} sequence and the resultant recombinant viruses we generated follow the "rule of six" (2). To investigate whether this is a requirement for FeMV, a minigenome, rFeMV^{US5}DIGluc, was generated that had the coding sequence for *Gaussia* luciferase (Gluc), as a reporter gene, surrounded by the FeMV^{US5} 3′ and 5′ noncoding termini. rFeMV^{US5}DIGluc adhered to the "rule of six". When tested in minigenome assays, this minigenome expressed a high level of Gluc activity (Fig. 3*C*, +L). When the L protein–expressing vector was omitted from the assay, three logs less Gluc activity was detected (Fig. 3*C*, −L), indicating that minigenome replication and transcription were necessary to produce the Gluc signal. rFeMV^{US5}DIGluc was modified by removing a second stop codon at the end of the Gluc open reading frame (ORF) to generate rFeMV^{US5}DIGluc + 3. rFeMV^{US5}DIGluc + 3 does not adhere to the "rule of six". When this minigenome was tested, Gluc activity was dramatically reduced (Fig. 3*C*, +L vs. −L), indicating that "rule of six" adherence is a requirement for efficient FeMV^{US5} replication.

FeMV Is a Cathepsin-Dependent Morbillivirus. Next, we investigated whether rFeMV^{US5}-induced cell-to-cell fusion was, like H and F glycoprotein–induced fusion, dependent on a cysteine protease. CRFK-feCD150 cells were infected with rFeMV^{US5}-Venus(6) in the presence of DMSO as a control, furin inhibitor I, cysteine protease inhibitor E64d, or cathepsin B/L inhibitor CA-074Me. After 5 d, the rFeMV^{US5}Venus(6) infection in the presence of DMSO or furin inhibitor I had spread significantly (Fig. 3 *D* and *E*). However, the infection was limited to single

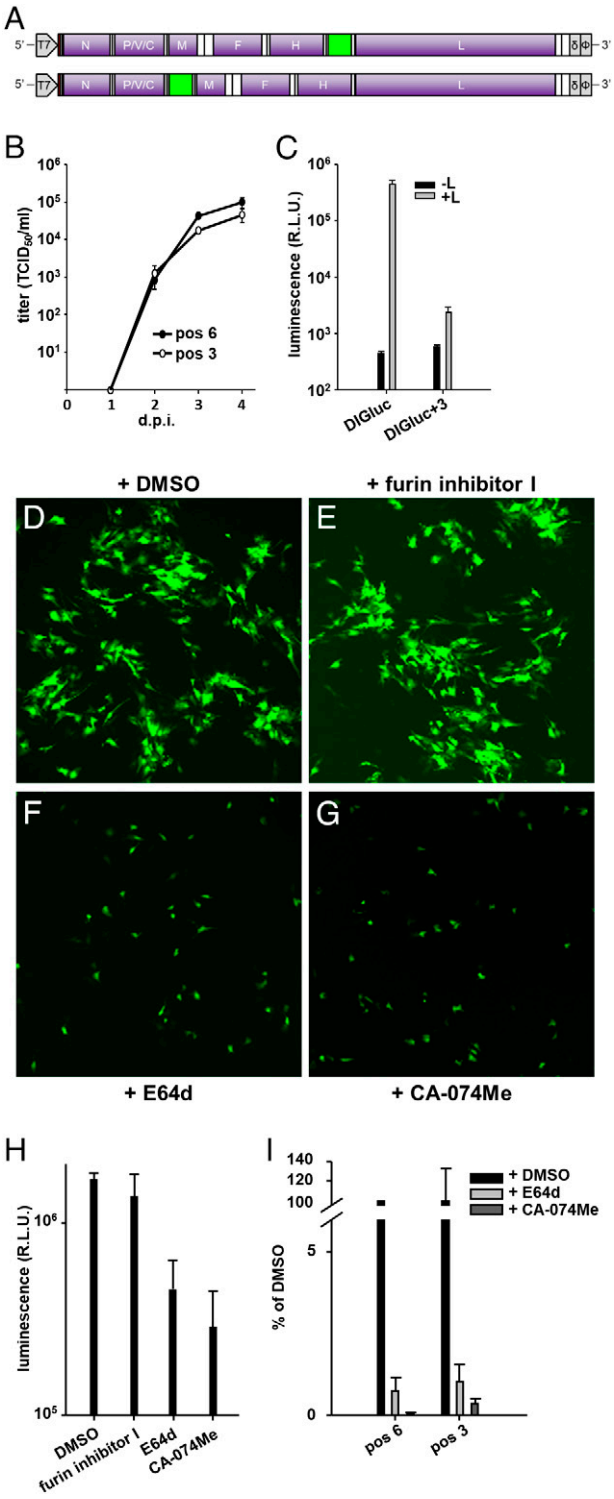

Fig. 3. rFeMV^{US5}-induced cell-to-cell fusion is inhibited by a cathepsin protease inhibitor. (*A*) Schematic representation of plasmids generated to allow recovery of rFeMV^{US5} expressing Venus from an ATU between the *H* and *L* genes [pFeMV^{US5}Venus(6); *Upper*] or *P* and *M* genes [pFeMV^{US5}Venus(3); *Lower*]. Coding sequences (purple), noncoding sequences (white), and intergenic trinucleotide (vertical black lines in noncoding sequences) are indicated. Genomes are surrounded by a T7 RNA polymerase promoter (T7), a hammerhead ribozyme (red boxes), a hepatitis delta ribozyme (δ), and T7 RNA polymerase terminator (φ) sequences to allow for recovery of RNA corresponding to the viral genomes from the plasmids. (*B*) Multistep growth analysis of rFeMV^{US5}Venus(6) (position [pos] 6) and rFeMV^{US5}Venus(3) (position [pos] 3) in CRFK-feCD150 cells over 4 d. Error bars represent one SEM for all curves ($n = 3$ for each virus). (*C*) Gluc activity in HEp-2 cells at 2 d post-transfection with p(−)FeMV^{US5}DIGluc (DIGluc; "rule of six" compliant) or p(−)FeMV^{US5}DIGluc + 3 (DIGluc + 3; not "rule of six" compliant), pCG-FeMV^{US5}N, and pCG-FeMV^{US5}P either with (+L) or without (−L) pCG-FeMV^{US5}L. (*D*–*G*) Representative photomicrographs depicting Venus fluorescence observed in CRFK-feCD150 cells 5 d after infection with rFeMV^{US5}Venus(6) in the presence of DMSO (*D*) or inhibitors: furin inhibitor I (*E*), E64d (*F*), or CA-074Me (*G*). (*H*) Luminescence (*y* axis; R.L.U.) detected 2 d after CRFK-feCD150 cells transfected with pCG-NrlucEGFP and infected with rFeMV^{US5}-Venus(6) in the presence of inhibitors were overlaid (in the presence of inhibitors) with a population of CRFK-feCD150 cells that had previously been transfected with pCG-rlucEGFPC. (*I*) Quantification of virus recovered 4 d after infection of triplicate CRFK-feCD150 monolayers with rFeMV^{US5}Venus(6) or rFeMV^{US5}Venus(3) in the presence of DMSO, E64d cysteine protease inhibitor, or CA-074Me cathepsin inhibitor. Titers determined in the presence of DMSO are set to 100%.

cells, with no spread from the initially infected cell in the presence of cysteine protease (Fig. 3*F*) or cathepsin (Fig. 3*G*) inhibitors. To quantify these differences, CRFK-feCD150 cells were transfected with pCG-NrlucEGFP; 24 h later, they were infected with rFeMV^{US5}Venus(6), and inhibitors were added. After another 24 h, these cells were overlaid (in the presence of inhibitor) with a population of CRFK-feCD150 cells that had been transfected with pCG-rlucEGFPC 48 h earlier. After incubation with inhibitors for 2 d, monolayers were assessed for luciferase activity (Fig. 3*H*). As expected, there was no difference in luciferase activity in cells treated with furin inhibitor vs. the DMSO control, whereas activity was reduced in cells treated with cysteine protease or cathepsin inhibitors.

Triplicate CRFK-feCD150 monolayers were infected with rFeMV^{US5}Venus(6) or rFeMV^{US5}Venus(3) in the presence of DMSO, E64d cysteine protease inhibitor, or CA-074Me cathepsin inhibitor. After 4 d, released virus was quantified (Fig. 3*I*). The presence of cysteine protease or cathepsin inhibitors reduced the infectious virus titers by two logs, indicating that the inhibitors prevented efficient assembly and egress of infectious virions.

FeMV Initially Causes a Typical Morbillivirus-Like Disease in the Natural Host. Nothing is known about the primary route of infection or disease progression of FeMV-infected animals. Cats were infected with rFeMV^{US5}Venus(6) and rFeMV^{US5}Venus(3). Animals were preimplanted (intraperitoneally) with a temperature data logger, and blood samples were collected every 2 d.p.i. until 14 d.p.i. At 7, 14, and 28 d.p.i., one cat was euthanized, and a full necropsy was performed to determine the acute-phase pathogenesis of the virus. Data loggers recorded an increase in body temperature after infection, peaking at 5 d.p.i. (Fig. 4*A*).

All animals developed lymphopenia early after infection (Fig. 4*B*). White blood cells (WBCs) were isolated from the blood samples, and the percentage of virus$^+$ (Venus$^+$) cells was determined by flow cytometry (Fig. 4*C*). All animals had detectable Venus$^+$ WBCs at 6 to 10 d.p.i., with concomitant virus isolation from these samples (Table 1), after which the infection cleared from the blood. At necropsy, Venus$^+$ cells could be detected in single-cell suspensions from lymph nodes and in the bronchoalveolar lavage (BAL) sample at 7 d.p.i. (Fig. 4*D*). By 14 d.p.i., Venus$^+$ cells were barely detectable in the BAL and were not detectable in the lymph nodes. Histopathological assessment of tissues collected at each necropsy confirmed disease and identified the peak of virus detection at 7 d.p.i. In the lungs, Venus protein and viral RNA could be detected in the interstitium (Fig. 4 *E* and *H* and *SI Appendix*, Fig. S4*A*), bronchial tissue (Fig. 4 *F* and *I* and *SI Appendix*, Fig. S4*B*), and bronchus-associated lymphoid tissue (Fig. 4 *G* and *J* and *SI Appendix*, Fig. S4*C*) at 7 d.p.i, and virus was isolated from lung tissue and BAL at this time point (Table 1).

FeMV Targets the Kidneys Later in Infection. In addition to the samples outlined above, urine samples were also collected from all living animals at 6, 12, and 21 d.p.i. and from all

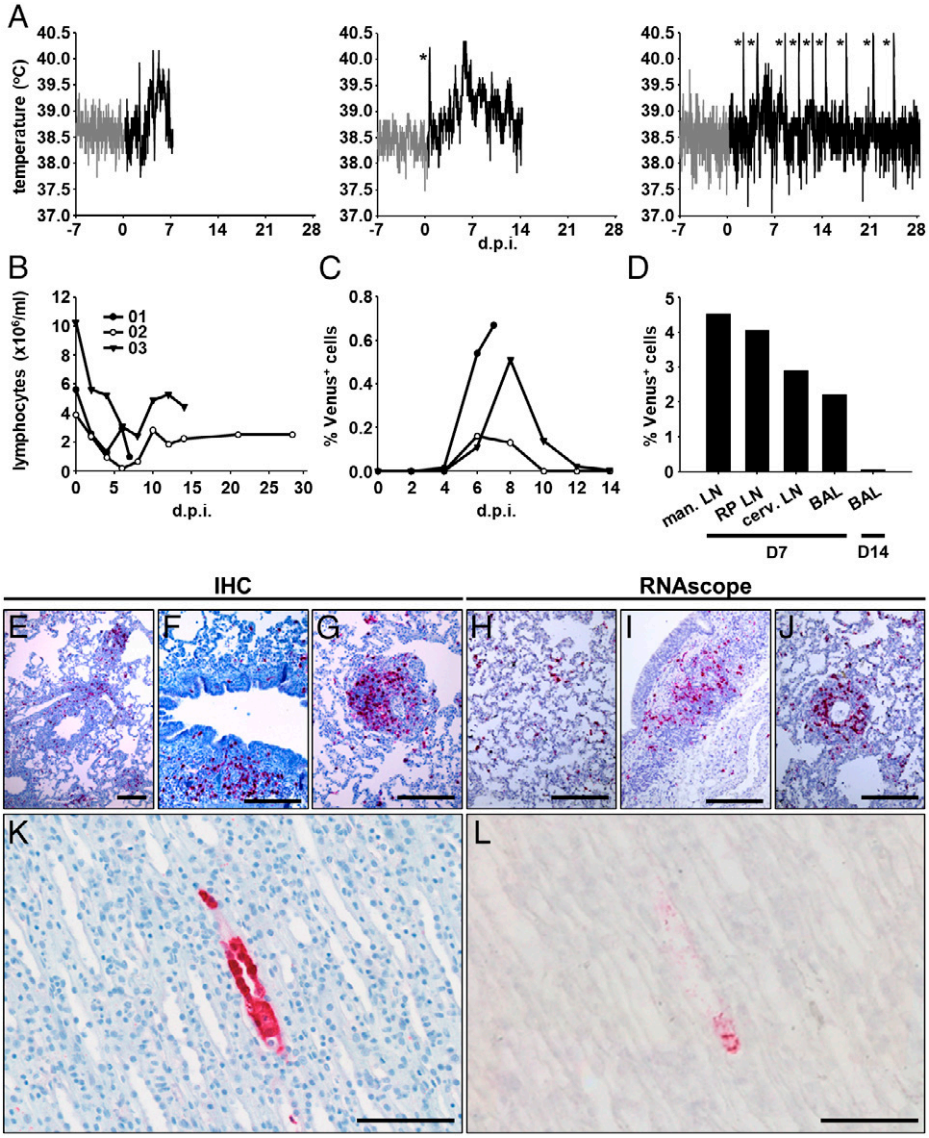

Fig. 4. rFeMV^{US5} causes a morbillivirus-like disease in the natural host. Infection of cats with rFeMV^{US5}Venus(6) and rFeMV^{US5}Venus(3) resulted in systemic disease. (*A*) Body temperature was measured every 10 min preinfection (gray) and postinfection (black) using an intraperitoneal data logger. Temperature data for cats euthanized at 7, 14, and 28 d.p.i. are depicted left to right. *Procedure related temperature spikes. (*B*) Lymphocyte numbers were measured in EDTA blood samples. Venus-positive cells were quantified by flow cytometry in purified WBC samples (*C*; symbols are the same as in *B*) and in cell samples dissociated from mandibular (man.), retropharyngeal (RP), and cervical (cerv.) lymph nodes (LNs) or prepared from BAL samples at 7 (D7) or 14 (D14) d.p.i. (*D*). (*E*–*J*) Virus distribution in cat lung tissue at 7 d.p.i. Visualized by immunodetection (IHC) of Venus protein (*E*–*G*; purple) or detection of virus genome (RNAscope) by ISH (*H*–*J*; purple) in formalin-fixed interstitial (*E* and *H*), peribronchial (*F* and *I*), and bronchus-associated lymphoid (*G* and *J*) tissue sections. (*K* and *L*) Detection of infected cells in renal medullary tubules at 28 d.p.i. Visualized by immunodetection (IHC) of Venus protein (*K*; purple) or detection of virus genome (RNAscope) by ISH (*L*; purple) in serial sections. (Scale bars: *E*–*J*, 200 μm; *K* and *L*, 100 μm.)

animals at necropsy. Virus was isolated from all animal 02 samples from 12 d.p.i. onward and from animal 03 at necropsy (14 d.p.i.) (Table 1). No virus was isolated from any animal urine at the earlier time point, when virus detection peaked in the WBCs (Fig. 4*C*) and in lymph nodes and BAL (Fig. 4*D*). Histopathological assessment of hematoxylin and eosin–stained kidney sections indicated the presence of lymphoplasmacytic lesions and pelvitis in the 14- and 28 d.p.i. sections but not in the 7 d.p.i. sections. Based on these observations, kidney sections were assessed for the presence of virus, with Venus protein (indicating infected cells) (Fig. 4*K*) and viral RNA (Fig. 4*L*) detected in medullary tubule epithelium in the 28 d.p.i. sections. Virus was not detected in the 7- or 14 d.p.i. sections.

Lymphoid Tissues Are Targeted during Acute rFeMV Infection. Three additional cats were infected with rFeMV^{US5}Venus(6) and rFeMV^{US5}Venus(3) to examine the peak of infection. Animals were preimplanted (subcutaneously) with a data logger, and blood samples were collected from all animals at 2, 5, and 6 d.p.i. and two animals at 7 d.p.i. All animals were euthanized at 7 d.p.i., and full necropsies were performed to characterize the acute-phase pathogenesis of the virus. Infections proceeded similarly, temperature increases peaked at 5 d.p.i. (Fig. 5*A*), and similar percentages of Venus^{+} cells were detected in the blood at equivalent time points (Fig. 5*B*).

Macroscopic imaging confirmed lymphotropism of the acute infection. All lymph nodes were highly infected (Fig. 5 *C* and *F*) with the thymus (Fig. 5 *C* and *D*) and tonsils (Fig. 5*E*) fluorescing brightly during macroscopic bioimaging. Multiplex fluorescence immunohistochemistry (IHC) in formalin-fixed, paraffin-embedded (FFPE) lung and lymph node tissues was performed to identify the infected cell populations. Antibodies

Table 1. Summary of d.p.i. when the virus was isolated from clinical samples

Animal	WBCs*	Throat and nose swabs†	Urine‡	BAL§	Lung§
01¶	4, 6, 7	—#	—#	7	7
02¶	8	—#	12, 21, 28	—#	—#
03¶	4, 6, 8, 10, 12, 14	—#	14‖	—#	—#

*Samples were collected from living animals at 2, 4, 6, 8, 10, 12, 14, and 21 d.p.i. and from each animal at necropsy.
†Samples were collected from living animals at 2, 6, 12, 17, and 21 d.p.i. and from animal 02 at necropsy.
‡Samples were collected from living animals at 6, 12, and 21 d.p.i. and from each animal at necropsy.
§Samples were collected at necropsy only.
¶Animals 01, 02, and 03 were euthanized at 7, 28, and 14 d.p.i., respectively.
#Virus was not isolated from any samples collected.
‖No sample was obtained at 12 d.p.i.

that are verified for use in cat tissue are limited, but we were able to identify B cell (CD20) and monocyte/macrophage (myeloid/histiocyte antigen) markers that were functional. An antibody against Venus was also included to mark infected cells. In all tissues examined, the majority of Venus$^+$ cells were monocytes/macrophages (Fig. 5 *G–K* and *SI Appendix*, Fig. S5); however, not all monocytes/macrophages were Venus$^+$. We did not readily identify Venus$^+$ B cells in any of the tissues examined.

Discussion

FeMV Uses feCD150 as an Entry Receptor. Based on a lack of conservation of residues known to be important for morbillivirus H glycoprotein interaction with CD150 (28–34), our hypothesis was that FeMV could not use CD150 as a receptor. However, when FeMV F and H glycoproteins were expressed in feCD150-positive cells, they caused cell-to-cell fusion (Fig. 1*B* and *SI Appendix*, Fig. S1). MV and CDV also bind feCD150 and induce cell-to-cell fusion. Similarly, rFeMV^{US5}Venus(6) and rFeMV^{US5}Venus(3) also required feCD150 expression to infect and spread in CRFK cells. When we attempted to analyze the growth kinetics of these viruses in CRFK cells lacking feCD150, they occasionally entered cells at very low efficiency. However, cell-to-cell spread was limited, and infectious virus was never recovered (*SI Appendix*, Fig. S6). The ability of wild-type FeMV to enter CRFK cells at low efficiency likely explains how some groups have been able to culture FeMV after prolonged "blind passage" in cells lacking a CD150 receptor (1, 11, 35, 36). This is presumably concomitant with the accumulation of adaptive mutations, which has been shown to occur during wild-type MV passage in Vero and chicken fibroblast cells (37–39) and led to adaption of that virus to use CD46 as a receptor (40, 41). Crucially, the virus that we based our reverse genetics system on was sequenced directly from a clinical sample (urine) and had never been isolated or passaged in laboratory cells; it is critical that such a virus, which has had no opportunity to adapt to alternative receptor usage, is used for the type of pathogenesis studies described in this manuscript.

FeMV Is a Unique Morbillivirus Employing a Cathepsin Protease for F Glycoprotein Processing. All paramyxovirus F glycoproteins are expressed first as an inactive precursor (F_0), which is processed proteolytically by the ubiquitous cellular protease furin (42) to produce disulfide-linked active F_1 and F_2 subunits. Processing exposes the hydrophobic fusion peptide, and biologically active F_1 and F_2 subunits in complex with the H glycoprotein are transported to lipid rafts on the plasma membrane where virions are assembled and budding occurs (43). Until the discovery of FeMV, all morbillivirus F glycoprotein sequences contained a polybasic cleavage signal at the predicted furin cleavage site. Alignment of the FeMV F glycoprotein sequences of FeMV, MV, and CDV identified the highly conserved hydrophobic fusion peptide at the end of F_1. However, surprisingly, an upstream polybasic signal was absent, and only a single basic residue was present at the predicted cleavage site.

It has been reported that FeMV uses a cellular trypsin-like protease to cleave F_0 at the monobasic cleavage signal (1). When we first performed fusion assays with the FeMV glycoproteins transfected into CRFK-feCD150 cells, we observed that the induction of cell-to-cell fusion did not require the addition of exogenous trypsin and that the addition of such protease did not enhance fusion; similarly, it was subsequently reported that the addition of trypsin during virus titration in CRFK cells did not augment the resultant virus titers (44). This suggested that F_0 was being cleaved efficiently using an endogenous protease expressed in the cells.

We used our quantitative dual bimolecular complementation assay in the presence of protease-specific inhibitors to show that, as expected, furin was not the protease responsible and that a cysteine protease was. The cysteine protease inhibitor E64d and cathepsin B/L inhibitor CA-074Me (45) also prevented cell-to-cell fusion and spread by the recombinant viruses rFeMV^{US5}Venus(6) and rFeMV^{US5}Venus(3) in CRFK-feCD150 cells. Replication of the viruses must occur in infected cells before green fluorescence can be detected. Thus, comparison of the foci of infection in Fig. 3*D* with the number of infected cells in Fig. 3 *F* and *G* shows that in the presence of E64d or CA-074Me, viruses can enter cells and initially replicate. The block in cell-to-cell fusion must occur due to the inability of *de novo* synthesized fusion protein to be cleaved and trafficked to the plasma membrane. These data also indicate that the F_0 glycoprotein is not cleaved during entry of the virus to the cell as is the case with, for example, Ebola virus (46) or some coronaviruses (47). Whether this feature, alongside the genetic distance from canonical morbilliviruses, will ultimately lead to FeMV being assigned to a new genus remains to be determined.

FeMV Infects Immune Cells in the Natural Host during the Early Stages of the Disease. Cats (*Felis catus*) are naturally infected by FeMV and are, therefore, the ideal species to examine FeMV infection, pathogenesis, and transmission. Initially, we inoculated three cats with FeMV-expressing fluorescent protein to examine the time course of infection. The ability of a virus to produce green fluorescence in infected cells is a powerful means to track virus spread in animals (48–51) and identify very small numbers of infected cells (52). Animals were euthanized at 7, 14, and 28 d.p.i. to examine spread of the virus over time and the tissues that are targeted. The sampling and necropsy time points were chosen based on our detailed understanding of the disease courses of CDV in ferrets (53) and MV in macaques (54). All animals showed an increase in temperature, peaking at 5 d.p.i., which is reminiscent of CDV-induced temperature increases in ferrets (53). Virus was detected in the WBCs, and animals developed lymphopenia, both hallmarks of morbillivirus disease in susceptible hosts (48, 49, 55, 56). In both the animals that remained alive after 7 d.p.i. the lymphocyte numbers recovered, although they did not reach preinfection levels during the time course of the experiment, a pattern also observed in MV and CDV infections. Lymphodepletion contributes to the long-term immunosuppression seen after morbillivirus infection

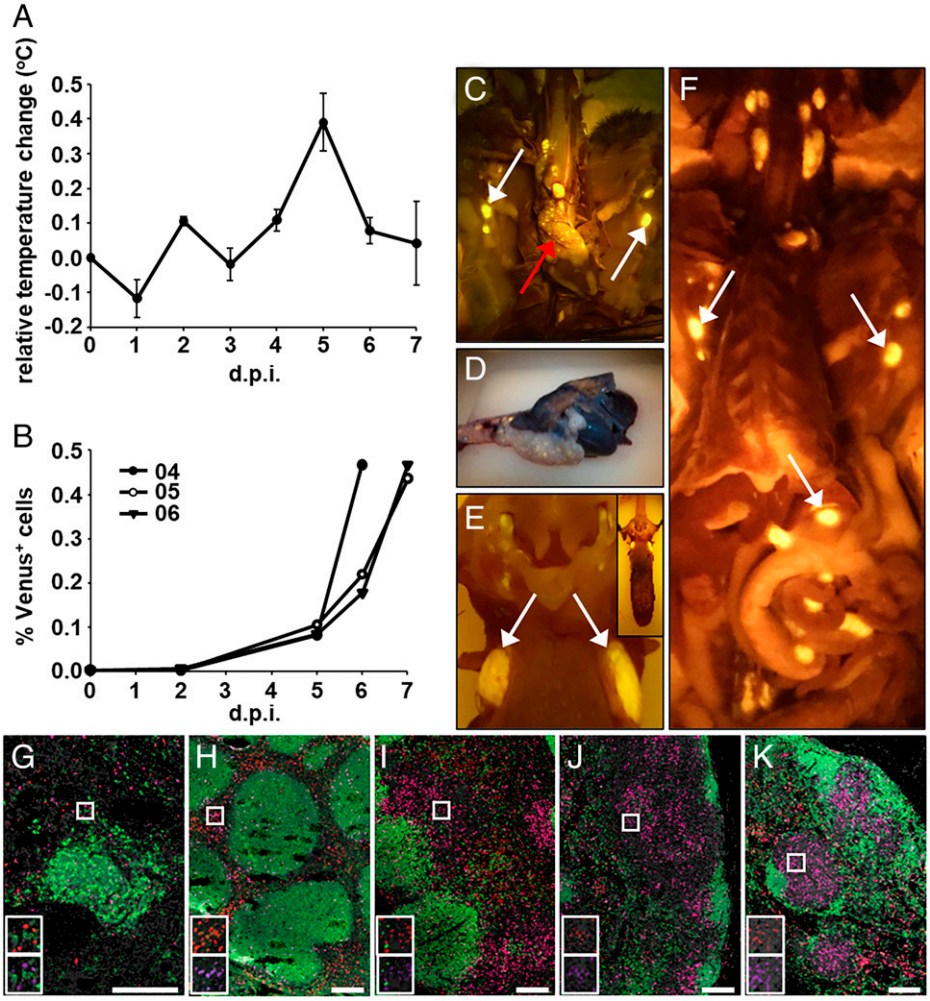

Fig. 5. Lymphoid tissues are targeted during acute rFeMV^{US5} infection. (*A*) Body temperature was measured every 5 min using a subcutaneous data logger. Temperatures for each d.p.i. were averaged and are displayed as the change in temperature relative to the average temperature for the 7 d preinfection (plotted as 0 d.p.i.). (*B*) Venus-positive cells were quantified by flow cytometry in purified WBC samples. (*C*–*F*) Macroscopic detection of Venus fluorescence in the thymus (*C*, red arrow, and *D*), lymph nodes (*C* and *F*; representative lymph nodes are marked with white arrows), tonsils (*E*, white arrows; tongue and tonsils are shown at a lower magnification in *E*, *Inset* for orientation), and other lymphoid tissues (*F*) at 7 d.p.i. *C* and *F* depict the same animal before (*C*) and after (*F*) removal of the thymus and upper respiratory tract. (*G*–*K*) Infected cell (Venus-positive; purple) phenotyping using antibodies against CD20 (B cells; green) and myeloid/histiocyte antigen (monocytes/macrophages; red) in the lung (*G*), tonsil (*H*), mesenteric lymph node (*I*), inguinal lymph node (*J*), and axillary lymph node (*K*). The areas marked by white boxes in the main triple-overlay image are shown at higher magnifications as red (monocytes/macrophages)/green (B cells) and purple (Venus-positive)/green (B cells) double-overlay images in *G*, *Inset*, *H*, *Inset*, *I*, *Inset*, *J*, *Inset*, and *K*, *Inset*. Nuclei are counterstained with 4′,6-diamidino-2-phenylindole (DAPI) (gray). (Scale bars: 200 μm.)

(56, 57). At peak, the percentage of Venus$^+$ WBCs was very low compared with those seen in MV-infected macaques (49, 58) and particularly, in CDV-infected ferrets (48, 53) where cell populations are decimated, leading to a propensity for secondary infections and frequent necessity to euthanize animals by 14 to 16 d.p.i (53). One possible explanation for this is the availability of cathepsin B in the peripheral blood cells; in humans, levels are extremely low in CD19$^+$ B cells and CD4$^+$ and CD8$^+$ T cells (http://biogps.org/#goto=genereport&id=1508), which are all major targets for MV and CDV in the animal models (48, 49). Cathepsin B levels are significantly higher in CD14$^+$ monocytes, which are present at much lower levels in the cat blood (2.4 to 7.1% at day 0) compared with the lymphocytes (40.9 to 45.8% at day 0). Monocytes are also significant target cells for MV in humans (59) that are not recapitulated in macaque infections (49). The low levels of infected cells in WBCs, even at the peak of acute infection, may also explain why other groups have been unsuccessful in detecting virus in blood samples (1, 8, 10, 35). Surprisingly, we did not isolate the virus from nose or throat swabs at any time point assayed; virus shedding from the respiratory tract peaks at 7 to 11 d.p.i. in MV-infected macaques (60) and increases during the second week of infection in CDV-infected ferrets (53). However, we isolated virus from urine at later time points.

At necropsy, virus was detected in cells purified from lymph nodes and a BAL sample at 7 d.p.i. Viral antigen and RNA were also both abundant in the lungs at this time point. Bronchi and bronchiole epithelium never displayed immunoreactivity/probe hybridization, and only rare alveolar type 1 pneumocytes were impacted, with the overwhelming majority of signal observed in perivascular, peribronchiolar, interstitial, and alveolar mononuclear infiltrates. Phenotyping the infected cells in the lymph nodes and lung indicated that the majority of the Venus$^+$-infected cells costained for the monocyte/macrophage marker, with minimal to absent costaining for the B cell marker. Unfortunately, we could not identify a specific T cell marker that worked efficiently in feline tissues. However, limited preliminary analysis and the localization of infected cells suggest that T cells are also not a major target for FeMV in lymphoid/lung tissues. These findings are at variance to what is seen in lymphoid tissue infection with MV in macaques and CDV in ferrets, where B and T cells are

abundantly infected (48, 49, 58). However, macrophages/dendritic cells were identified as a major target for MV in the lung (49, 58). Interestingly, it was previously shown that a feline macrophage cell line, Fcwf-4, was highly susceptible to FeMV (35), and we have corroborated this by infection of these cells with rFeMV^{US5}Venus(3) (*SI Appendix*, Fig. S7). IHC performed on lymph node sections from naturally infected FeMV^{+} cats also identified infected macrophages (1, 61). It has previously been shown that feline primary pulmonary epithelial cells are susceptible to a closely related FeMV *in vitro* (35). Our *in vivo* study extends this observation, showing that although some FeMV-infected pneumocytes could be detected in the lung (*SI Appendix*, Fig. S4*A*), we did not observe the extensive alveolar epithelium disruption reported for MV (60), which could explain why we did not isolate virus from the nose and throat swabs.

Urine Is Likely to Play a Major Role in FeMV Host-to-Host Transmission. FeMV was originally detected in and isolated from cat urine samples (1). As expected, we were able to isolate virus from the urine of cats infected with rFeMV^{US5}. rFeMV^{US5} was shed in the urine from 12 d.p.i. and was still present at necropsy in the urine of the one cat that was allowed to progress to 28 d.p.i. Virus could not be isolated from any cat urine sample collected at 6 d.p.i. MV can also be isolated from the urine of measles patients after the appearance of rash (62), and CDV can be detected in the urine of naturally infected dogs (63, 64), where it is present at high viral load (63). At necropsy, we detected rFeMV^{US5} in the renal medullary tubule epithelium by IHC and corroborated this by detecting RNA in a serial section. This detection is in good agreement with analysis of kidney sections from naturally infected cats, where the FeMV antigen was detected in renal tubular cells (1, 61, 65). It has also been previously shown that feline primary kidney cells are susceptible to FeMV and that epithelial cells are the primary target (35). The facts that infectious FeMV can be readily isolated from cat urine for a prolonged period [16 d in this study to months (35)] and that we did not isolate virus from nose or throat swabs at any time in our study raise the intriguing questions of how FeMV is transmitted and whether this differs from the respiratory transmission used by other morbilliviruses. Although this study was focused on understanding FeMV primary pathogenesis receptorology, we have performed a preliminary analysis for usage of the second morbillivirus (epithelial) receptor nectin-4 (66, 67). Like CD150, FeMV^{US5} H glycoprotein lacks the majority of conserved amino acids shown to be important for morbillivirus H glycoprotein/nectin-4 binding and/or function, but all the amino acids in nectin-4 shown to be important for these functions are completely conserved (29, 68–71). Further studies will be required to confirm if nectin-4 acts as a receptor for FeMV and whether the potential for alternative receptor usage contributes to the excretion of the virus in the urine rather than from the respiratory tract.

In these studies, we have shown that FeMV uses feCD150 as a cellular receptor and employs a unique protease for F glycoprotein processing. Our fluorescent protein–expressing rFeMV has been used to illuminate viral pathogenesis in the cat following infection by a natural route. These approaches and viruses pave the way to determine the role that FeMV may have in the development of CKD, the leading cause of morbidity and mortality in older cats.

Materials and Methods

Cells. The CRFK epithelial cell line and the feline macrophage cell line Fcwf-4 were obtained from ATCC and grown in Eagle's minimum essential medium (ATCC) supplemented with 10% (vol/vol) fetal bovine serum (Thermo Fisher Scientific). The CRFK-feCD150 and CRFK-hCD150 derivative cells were grown in the same medium with periodic passage in the presence of puromycin (500 μg/mL) to maintain expression of CD150. HEp-2 cells were grown in Opti-MEM I supplemented with 3% (vol/vol) fetal bovine serum (both Thermo Fisher Scientific); 293T cells were purchased from ATCC and grown in advanced minimal essential medium supplemented with 10% (vol/vol) fetal bovine serum (both Thermo Fisher Scientific).

Generation of CRFK-feCD150 and CRFK-hCD150 Stable Cell Lines. DNA strings encoding feCD150 (accession no. NM_001278826) or hCD150 (accession no. NM_003037.5) were synthetically generated (GeneArt Gene Synthesis; Thermo Fisher Scientific) and cloned into a lentiviral expression vector, which also encoded puromycin resistance to generate pHAGE^{puro}-feCD150 and pHAGE^{puro}-hCD150. pHAGE^{puro}-feCD150 or pHAGE^{puro}-hCD150, helper plasmids expressing HIV-gag and pol, and vesicular stomatitis virus (VSV) glyco- (G) protein (VSV-G) were cotransfected into 293T cells using lipofectamine 2000 (Thermo Fisher Scientific). Lentivirus-containing supernatants were collected every 12 h for 2 consecutive days starting at 48 h posttransfection (h.p.t.). The supernatants were pooled and filtered through a sterile 0.45-μm filter (Millipore) to remove any residual cells. The lentiviral particles were concentrated by centrifugation through 20% (wt/vol) sucrose at 28,000 × *g* for 2 h at 4 °C. The pellet was resuspended in 200 μL phosphate buffered saline (PBS, Thermo Fisher Scientific), and 20 μL were used to transduce 5×10^5 CRFK cells seeded in a six-well culture plate in the presence of polybrene (5 μg/mL; Sigma Aldrich). Cells were then selected using puromycin (5 μg/mL; Thermo Fisher Scientific) 2 d after the transduction.

Plasmids. The F and H glycoprotein sequences of FeMV^{US1} (17), FeMV^{US2} (accession nos. ON783815 and ON783816), and FeMV^{US5} and the N, P, and L protein sequences of FeMV^{US5} were generated by PCR and cloned into the eukaryotic expression vector pCG (72) using unique *Asc* I and *Afe* I restriction sites to generate pCG-FeMV^{US1}F, pCG-FeMV^{US1}H, pCG-FeMV^{US2}F, pCG-FeMV^{US2}H, pCG-FeMV^{US5}F, pCG-FeMV^{US5}H, pCG-FeMV^{US5}N, pCG-FeMV^{US5}P, and pCG-FeMV^{US5}L. pCG-FeMV^{US5}F was modified by insertion of a PCR-generated insert containing an AU1 epitope tag at the carboxyl (C) terminus of FeMV^{US5}F between unique *Eco*R V and *Afe* I restriction sites to generate pCG-FeMV^{US5}F$_{AU1}$. A synthetically generated gene string (GeneArt Gene Synthesis) containing a polybasic cleavage signal at the original monobasic cleavage site in FeMV^{US5}F was used to modify pCG-FeMV^{US5}F$_{AU1}$ by cloning between unique *Asc* I and *Bsr*G I restriction sites to generate pCG-FeMV^{US5}F$_{PB\text{-}AU1}$. The F and H glycoprotein sequences of MV^{KS} (52) and CDV^{RI} (73) and the F and G glycoprotein sequences of NiV (74) were generated by PCR and cloned into pCG using unique *Asc* I and *Spe* I restriction sites to generate pCG-MV^{KS}F, pCG-MV^{KS}H, pCG-CDV^{RI}F, pCG-CDV^{RI}H, pCG-NiV^{MA}F, and pCG-NiV^{MA}G. Sequences for NrlucEGFP and rlucEGFPC were amplified from plasmid templates (75, 76) by PCR and cloned into pCG using unique *Mlu* I and *Pst* I restriction sites to generate the pCG-NrlucEGFP and pCG-rlucEGFPC plasmids used in the bimolecular fluorescence complementation assay. The sequence for FeMV^{US5}DIGluc was generated synthetically (GeneArt Gene Synthesis) and cloned into a modified pBluescript plasmid (77) using unique *Nar* I and *Not* I restriction sites to generate p(−)FeMV^{US5}DIGluc. This contains a Gluc ORF flanked by the FeMV^{US5} 3′ and 5′ noncoding termini and surrounded by a T7 RNA polymerase promoter downstream and by a hepatitis delta virus ribozyme and T7 terminator sequences upstream. A synthetically generated gene string (GeneArt Gene Synthesis) was used to modify p(−)FeMV^{US5}DIGluc by removing an extra stop codon after the Gluc ORF and was cloned using unique *Nco* I and *Bsr*G I restriction sites to generate p(−)FeMV^{US5}DIGluc + 3. Both plasmids produce negative-sense minigenome transcripts upon T7 RNA polymerase transcription.

Inhibitors. The cysteine protease inhibitor, E64d (Sigma-Aldrich), was used at a concentration of 20 μM. The cell-permeable cathepsin B/L inhibitor, CA-074Me (Calbiochem), was used at a concentration of 10 μM. The furin inhibitor, furin inhibitor I (Calbiochem), was used at a concentration of 50 μM. All inhibitors were dissolved in sterile DMSO. For fusion assays, inhibitors were added after the transfection of glycoprotein-expressing plasmids. For virus assays, inhibitors were added with the virus inoculum. In both cases, controls containing the same

volume of DMSO were included, and fresh inhibitor/DMSO was supplied with media changes.

Bimolecular Fluorescence Complementation Assay. This assay is based on the previously published self-associating split green fluorescent protein (GFP) (76, 78). Subconfluent CRFK cells in six-well trays were transfected with 1 μg each of pCG-NrlucEGFP and plasmids encoding homologous pairs of glycoproteins. Separate wells of CRFK cells (for controls) or CRFK-feCD150 or CRFK-hCD150 cells were transfected with pCG-rlucEGFPC. At 18 h.p.t., all cells were trypsinized and mixed in appropriate combinations before reseeding in six-well trays and further incubation. Cells were observed using a DMI3000B inverted microscope, and images were acquired using a DFC345 FX camera and LAS software (all Leica Microsystems) when sufficient green fluorescence was detected (at 48 to 72 h.p.t.). At this point, the growth medium was removed, the cells were washed once with PBS (1 mL), and 1× lysis buffer (500 μL; *Renilla* Luciferase assay system; Promega) was added before scraping the cells into the supernatant. The cell lysates were collected into 1.5-mL microcentrifuge tubes, and supernatants were collected by centrifugation at 6,000 rpm for 1 min. The supernatants were assayed by the addition of 1 μL (diluted in 49 μL of lysis buffer) to 50 μL of rLuc substrate (*Renilla* Luciferase assay system; Promega) followed immediately by light quantification using a LUMIstar Omega luminometer (BMG Labtech). The resulting luciferase activity is expressed as relative light units (R.L.U.).

For assays with virus, separate populations of CRFK-feCD150 cells were transfected (Lipofectamine 2000; Life Technologies) with pCG-NrlucEGFP or pCG-rlucEGFPC (1 μg plasmid per 10^6 cells); 24 h later, cells transfected with pCG-NrlucEGFP were infected with rFeMV^{US5}Venus(6) at a multiplicity of infection (M.O.I.) of 0.1. Infection was performed in the presence of inhibitors. After 24 h, these cells were overlaid (in the presence of inhibitor) with the population of CRFK-feCD150 cells that had been transfected with pCG-rlucEGFPC. After incubation with inhibitors for 2 d, monolayers were assessed for luciferase activity as described above for glycoprotein assays.

Sample Preparation, Polyacrylamide Gel Electrophoresis, and Western Blotting. CRFK-feCD150 cells were transfected with pCG-FeMV^{US5}F, pCG-FeMV^{US5}F$_{AU1}$, or pCG-FeMV^{US5}F$_{PB\text{-}AU1}$ in the absence or presence of the pancysteine protease inhibitor E64d. At 2 days posttransfection (d.p.t.), cell lysates were prepared. Medium was removed, and the monolayers were rinsed twice with 1 mL cold Dulbecco's (D)-PBS. Cold 1× radioimmunoprecipitation assay (RIPA) buffer (Boston Bioproducts; 200 μL) containing 1× HALT™ protease inhibitors (Thermo Fisher Scientific) was added to the monolayers and incubated on ice for 15 min. Monolayers were scraped into the buffer and transferred to cold 1.5-mL tubes. Lysates were incubated on ice for 30 min with intermittent vortexing before being centrifuged at 14,000 × *g* for 15 min at 4 °C to pellet nuclei. The cleared supernatants were used to prepare samples for polyacrylamide gel electrophoresis (PAGE) by adding appropriate volumes of 4× NuPAGE LDS sample loading buffer and ×10 NuPAGE reducing agent (both Thermo Fisher Scientific). PAGE samples were heated to 70 °C for 10 min before separation of proteins on a 10% NuPAGE bis-tris(hydroxymethyl)aminomethane polyacrylamide gel using the Xcell SureLock Mini-Cell system (Thermo Fisher Scientific) according to the manufacturer's instructions. An aliquot of SeeBlue Plus2 Protein Standard (Thermo Fisher Scientific) was included on each gel to allow for estimation of protein sizes. Proteins were transferred to nitrocellulose using an iBlot (standard 7 min at 20 V transfer protocol; Thermo Fisher Scientific) according to the manufacturer's instructions. Blots were blocked for 1 h in Odyssey blocking buffer (PBS; LI-COR). Blots were incubated with primary antibodies (rabbit anti-AU1, 1:1,000, Novus Biologicals and mouse anti–β-actin, 1:5,000, Abcam; diluted in 50:50 Odyssey blocking buffer: PBS containing 0.2% [vol/vol] Tween-20) overnight at 4 °C.

Primary antibodies were removed, and blots were washed three times for 15 min with excess PBS. Blots were incubated with secondary antibodies (goat anti-rabbit 680, 1:10,000 and goat anti-mouse 800, 1:10,000, both LI-COR; diluted in 50:50 Odyssey blocking buffer: PBS containing 0.2% [vol/vol] Tween-20) with rocking for 1 h at room temperature. Secondary antibodies were removed, and blots were washed three times for 15 min with excess PBS before imaging using an Odyssey CLx (LI-COR) according to the manufacturer's instructions.

Minigenome Assays. HEp-2 cells were grown to 80% confluency in 24-well trays, rinsed with Opti-MEM I (1 mL; Thermo Fisher Scientific), and infected with MVA-T7 at an M.O.I. of one for 45 min. Lipofectamine 2000 (Thermo Fisher Scientific) was diluted with Opti-MEM I according to the manufacturer's instructions and incubated at room temperature for 10 min. A DNA mixture containing pCG-FeMV^{US5}N, pCG-FeMV^{US5}P, and pCG-FeMV^{US5}L eukaryotic expression plasmids and either p(−)FeMV^{US5}Gluc or p(−)FeMV^{US5}Gluc + 3 was added, and liposome–DNA complexes were formed by incubation for 20 min at room temperature. The MVA-T7 inoculum was removed, and the complexes were spotted onto the HEp-2 cell monolayers. Opti-MEM I (1 mL) was added to each well. After 18 h of incubation at 37 °C, the complexes were replaced with Opti-MEM I (1 mL) containing 3% (vol/vol) fetal bovine serum (Thermo Fisher Scientific). Supernatant samples were collected at 48 h.p.t. and were assayed by the addition of 100 ng native coelenterazine substrate (Nanolight Technologies) in D-PBS (Thermo Fisher Scientific) followed immediately by light quantification using a LUMIstar Omega luminometer (BMG Labtech). The resulting Gluc activity is expressed as R.L.U.

FeMV^{US5} Sequence Determination. A urine sample was collected by cystocentesis from a male neutered healthy pet domestic shorthair cat. All RNA extraction, cDNA synthesis, and PCR were performed in a clean room using dedicated pipettes, kits, enzymes, primers, and plasticware. cDNA synthesis and PCRs were set up using different pipettes. A reverse-transcriptase negative control was included to demonstrate that amplicons were not attributable to contamination. No tube that might contain an FeMV amplicon was ever opened in the clean room. All DNA gel electrophoresis was performed in a separate laboratory on a different floor.

Total RNA was extracted using a Viral RNA Minikit (Qiagen), and cDNA was prepared using SuperScript III reverse transcriptase (Thermo Fisher Scientific) priming with random hexamers. Screening (17) identified the sample as positive for FeMV RNA. Primers (*SI Appendix*, Table S2) were used to generate additional cDNAs from the extracted total RNA and generate PCR amplicons, which were either purified using a QIAquick PCR purification kit (Qiagen) or gel extracted and purified using a QIAquick gel extraction kit (Qiagen) before sequencing (Genewiz) with the same primers used to amplify the target region. Initially, primers (*SI Appendix*, Table S2, Asia and 776U designations) were designed using alignments of published FeMV sequences to identify highly conserved regions. Once the FeMV^{US5} sequence was available from these amplicons, FeMV^{US5}-specific primers (*SI Appendix*, Table S2, U122 and US5 designations) were designed for cDNA synthesis, PCR, and sequencing. Rapid amplification of cDNA ends was used to generate amplicons containing leader and trailer sequences as previously described (79); these were sequenced to determine the authentic genomic termini of FeMV^{US5}. Sequences were aligned in DNAstar SeqMan Pro software (Lasergene), and contigs were generated corresponding to the consensus sequence. DNAstar SeqBuilder software (Lasergene) was used to assemble and annotate the complete genome sequence. The complete FeMV^{US5} sequence is available with accession number MN604235.

Generation of Full-Length Clones and Recombinant Virus. Large amplicons from the FeMV^{US5} sequence determination were modified to incorporate an A overhang using Taq DNA Polymerase (Thermo Fisher Scientific) and subcloned using the TOPO TA Cloning Kit for Subcloning (Thermo Fisher Scientific). Clones were sequenced (Genewiz) to identify those that matched the consensus FeMV^{US5} sequence. A cloning strategy was devised based on available cloned DNA and unique restriction sites. A subclone was generated containing some viral sequences and the restriction sites necessary for the cloning strategy in a modified pBluescript vector (80). The full-length pFeMV^{US5} plasmid was generated by stepwise modifications of this subclone by insertion of sequences from the TOPO-cloned fragments using the appropriate subclone restriction sites.

To make pFeMV^{US5}Venus(3) and pFeMV^{US5}Venus(6), one of the TOPO-cloned fragments used in the generation pFeMV^{US5} was modified with synthetic DNA (GeneArt Gene Synthesis) to insert an ATU encoding Venus fluorescent protein between the *P* and *M* genes [pFeMV^{US5}Venus(3)] or *H* and *L* genes [pFeMV^{US5}-Venus(6)]. Appropriate restriction sites were used to switch the modified TOPO-cloned fragment containing the ATU into pFeMV^{US5}.

CRFK-feCD150 cells were infected with recombinant vaccinia virus MVA-T7 for 1 h at 37 °C. Inoculum was aspirated, and cells were transfected (Lipofectamine 2000; Life Technologies) with pCG-FeMV^{US5}N, pCG-FeMV^{US5}P, pCG-FeMV^{US5}L, and pFeMV^{US5}Venus(6) or pFeMV^{US5}Venus(3). After 18 h, the transfection mix

was removed and replaced with Eagle's minimum essential medium (ATCC) containing 10% (vol/vol) fetal bovine serum (Life Technologies). Cells were incubated for 5 to 7 d at 37 °C with 5% (vol/vol) CO_2. The presence of virus was confirmed by the cytopathic effect observed by phase-contrast microscopy and fluorescent microscopy. Virus stocks were prepared by trypsinizing cells in a virus-positive well and expanding to a T75 flask; when the cytopathic effect was maximal, monolayers were subjected to one freeze–thaw cycle, and debris was removed by centrifugation at 3,000 rpm for 10 min at 4 °C. The cleared supernatant (virus stock) was aliquoted and titrated in CRFK-feCD150 cells; calculated quantities, expressed in tissue culture infectious dose $(TCID)_{50}$ units (81), were used to calculate M.O.I.s for infections. Large volumes of virus stock were prepared in the presence of ruxolitinib (Thermo Fisher Scientific; 0.5 to 2.0 μM/mL) to enhance the virus production (82). The virus stock was then subjected to high-speed centrifugation through 20% (wt/vol) sucrose (Sigma) to generate purified virus stock for animal infections. Purified stocks were titrated as above.

Multistep Growth Analysis. CRFK-feCD150 cells in suspension were infected with rFeMV^{US5}Venus(6) or rFeMV^{US5}Venus(3) in triplicate at an M.O.I. of 0.1 for 4 h at 37 °C. The cells were spun out of the inoculum at 700 × *g* for 5 min, the pellet was resuspended, and the cell suspension was divided into aliquots in 36-mm-diameter wells (5×10^5 cells/well). At each indicated time point, the cells and medium were combined into a tube and subjected to one freeze–thaw cycle to release total virus. Virus present in the sample for each time point was determined by end-point titration in CRFK-feCD150 cells, and quantities are expressed in $TCID_{50}$ units/mL (81).

Animal Study Design. Animal experiments were conducted in compliance with all applicable US federal policies and regulations and Association for Assessment and Accreditation of Laboratory Animal Care (AAALAC) International standards for the humane care and use of animals. Protocols were approved by the Boston University Institutional Animal Care and Use Committee. Animals were housed in groups, and cages contained appropriate sources of environmental enrichment. Animals were observed several times per day, and all procedures were performed under light anesthesia using ketamine, medetomidine, and butorphanol followed by atipamezole reversal after handling. To determine the peak of infection, three 16- to 17-wk-old male domestic shorthair cats were infected with rFeMV^{US5}Venus(6) and rFeMV^{US5}Venus(3) (10^6 $TCID_{50}$ each intratracheal and 2×10^5 $TCID_{50}$ each intranasal). Twenty days prior to infection, cats were implanted (intraperitoneally) with data loggers programed to record core temperature every 10 s. Surgery sites were examined frequently and were fully healed prior to infection. Samples were collected from all living animals at various time points. Small blood samples were collected 2, 4, 6, 8, 10, 12, 14, and 21 d.p.i. Urine samples were collected 6, 12, and 21 d.p.i., and throat and nose swabs were collected 2, 6, 12, 17, and 21 d.p.i. Individual animals were euthanized at 7, 14, and 28 d.p.i., and full necropsies were performed. To further examine and confirm the peak of infection, three 16- to 17-wk-old male domestic shorthair cats were infected with rFeMV^{US5}Venus(6) and rFeMV^{US5}Venus(3) (10^6 $TCID_{50}$ each intratracheal and 2×10^5 $TCID_{50}$ each intranasal). Twenty days prior to infection, cats were implanted (subcutaneously) with data loggers programed to record temperature every 5 s. Small blood samples were collected 2, 5, 6, and 7 d.p.i. All animals were euthanized 7 d.p.i., and full necropsies were performed.

Samples and Assays. Small blood samples were collected in Vacuette tubes containing ethylenediaminetetraacetic acid (EDTA) as the anticoagulant. Before further processing, 50 μL were analyzed on a VetScan HM5 (Abaxis) using cat-specific parameters according to the manufacturer's instructions. Red blood cells (RBCs) were lysed in the remaining sample using ×1 multispecies RBC lysis buffer (eBioscience), and the remaining WBCs were collected by centrifugation (350 × *g* for 10 min), washed three times with D-PBS (Thermo Fisher Scientific), and resuspended in an appropriate volume of D-PBS based on pellet size. The WBCs were used directly for flow analysis using an LSRII flow cytometer (BD Biosciences). Venus protein fluorescence was detected in cells by excitation of the fluorophore with a Blue (488-nm) laser and detection using the Octagon detector array and fluorescein isothiocyanate parameter (using the 505 long pass mirror and a 530/30 band pass filter). The WBCs were also used for virus isolations by coculture with CRFK-feCD150 cells and screening for the development of Venus fluorescent protein. Urine samples were collected by cystocentesis; a 22- to 24-gauge (1- to 1.5-in) needle was used to enter the bladder percutaneously to withdraw a sample of up to 5 mL (maximum) of urine. Urine (1 mL) was directly used to inoculate confluent monolayers of CRFK-feCD150 in six-well trays. The inoculum was allowed to adsorb for 2 h at 37 °C before removal. Monolayers were washed twice before the addition of 2 mL CRFK medium. Monolayers were screened for the development of Venus fluorescent protein. Nose and throat swabs were collected into 1 mL virus transport medium. The medium was used directly for virus isolation by titration on CRFK-feCD150 cells in 96-well trays and screening for the development of Venus fluorescent protein.

At necropsy, tissues were collected directly into formalin for fixation and subsequent pathological processing and assessment. Lymph nodes were also collected into D-PBS for subsequent preparation of single-cell suspensions. Fatty tissue was removed from the lymph nodes, which were dissected into small pieces and added to gentleMACS dissociation C tubes (Miltenyi Biotec) containing advanced Roswell Park Memorial Institute (RPMI) medium supplemented with 10% (vol/vol) fetal bovine serum, 1% (vol/vol) Glutamax, and ×1 antibiotic–antimycotic (all Thermo Fisher Scientific). Samples were dissociated using a gentleMACS Dissociator (Miltenyi Biotec) set to the m_spleen_C preset parameter and transferred through 100-μm Falcon Cell Strainers into 50-mL centrifuge tubes (Thermo Fisher Scientific). The dissociated cells were collected by centrifugation (350 × *g* for 10 min), washed once with D-PBS (Thermo Fisher Scientific), and resuspended in an appropriate volume of D-PBS based on pellet size. The dissociated cells were used directly for flow analysis as above for WBCs. BAL samples were collected by insertion of an appropriately sized nasogastric tube into a primary mainstem bronchus and instillation of 10 to 15 mL of sterile saline using an attached syringe followed by rapid retraction of as much saline as possible. BAL cells were collected by centrifugation (350 × *g* for 10 min), washed once with D-PBS (Thermo Fisher Scientific), and resuspended in an appropriate volume of D-PBS based on pellet size. The cells were used directly for flow analysis and virus isolation as above for WBCs.

Macroscopic Detection of Venus Fluorescence. To examine fluorescence in the body cavity, the area was illuminated with a custom-made lamp containing six light emitting diodes (LEDs) with peak emission of 490 to 495 nm and viewed through amber glasses, which transmitted green light. Images were acquired using an iPhone 8 (Apple) and amber filter.

Chromogenic IHC. Tissues were stained immunohistochemically to detect the presence of Venus protein (surrogate of viral infection) in affected tissues. IHC was performed by an automated Ventana BenchMark ULTRA platform; 5-μm sections were deparaffinized in a xylene bath and rehydrated through graded ethanol solutions. Antigen retrieval was completed for 36 min at 95 °C using ULTRA CC1 (Roche); 100 μL of rabbit polyclonal anti-green fluorescent protein diluted at 1:400 (A11122; Invitrogen) was incubated on each slide at 37 °C for 32 min. Venus is a red-shifted variant of GFP, with only nine amino acid changes to that of GFP; furthermore, GFP antibodies are pan-GFP variant. One hundred microliters UV Red UNIV MULT (Roche) was dispensed onto each slide and incubated for 12 min at 36 °C. One hundred microliters of UV Red Enhancer (Roche) was dispensed onto each slide and incubated for 4 min at 36 °C. One hundred microliters each of UV Fast Red A and UV Red Naphthol (Roche) were dispensed onto each slide and incubated for 8 min at 36 °C. One hundred microliters of UF Fast Red B (Roche) was dispensed onto each slide and incubated for 8 min at 36 °C. One hundred microliters Hematoxylin II (Roche) was dispensed onto each slide and incubated for 8 min. One hundred microliters Bluing Reagent (Roche) was dispensed onto each slide and incubated for 8 min. All washes in between steps were completed with ready to use reaction buffer (Roche). Slides were removed from the autostainer, rinsed with water and Dawn dishwashing detergent, and dehydrated through graded alcohols and xylene. Slides were coverslipped using an automated coverslipper and coverslipping film. A lung section from a cat determined to no longer have systemic infection was used simultaneously as a negative control for EGFP.

Chromogenic In Situ Hybridization. *In situ* hybridization (ISH) targeting viral Venus messenger (m) RNA was performed on FFPE tissues using the RNAscope 2.5 high-definition RED kit (Advanced Cell Diagnostics) according to the manufacturer's instructions. Briefly, 14 probe pairs targeting the Venus gene were designed and synthesized by Advanced Cell Diagnostics (493891; Advanced Cell Diagnostics). After deparaffinization with xylene, a series of ethanol washes, and

peroxidase blocking, sections were heated in Antigen Retrieval Buffer (Advanced Cell Diagnostics) and then digested by proteinase plus (Advanced Cell Diagnostics). Sections were exposed to ISH target probe and incubated at 40 °C in a hybridization oven (HybEZ; Advanced Cell Diagnostics) for 2 h. After rinsing, the ISH signal was amplified using company-provided preamplifier and amplifier conjugated to alkaline phosphatase and incubated with a red substrate–chromogen solution for 10 min at room temperature. An *F. catus*–specific probe targeting the PPIB gene (455011; Advanced Cell Diagnostics) and a *Bacillus subtilis* probe targeting the DApB gene (310043; Advanced Cell Diagnostics) were utilized as positive and negative controls, respectively. Sections were then counterstained with hematoxylin, air dried, and coverslipped.

Multiplex fluorescent IHC. Tissue sections (5-μm) were baked at 60 °C for an hour and deparaffinized with xylene and a graded series of ethanol. Antigen retrieval was conducted using a Decloacking chamber (Biocare Medical) at 90 °C for 15 min in AR6 buffer (Akoya Biosciences). Multiplex fluorescent immunostaining was conducted following the Opal four-color user manual (Akoya Biosciences), including a nuclear 4′,6-diamidino-2-phenylindole (DAPI) counterstain. A tracheobronchial lymph node from a cat determined to no longer have systemic infection was used simultaneously as a negative control for GFP and a positive control for myeloid/histiocytic antigen and CD20. Whole-slide images were acquired using a Zeiss Axio Scan Z.1 whole-slide scanner at 200× equipped with a Colibri 7 LED light source and 16-bit Orcha Flash 4.0 monochrome camera. Immunohistochemical and acquisition parameters are outlined in *SI Appendix*, Table S3.

Data, Materials, and Software Availability. All study data are included in the article and/or *SI Appendix*.

ACKNOWLEDGMENTS. We thank Dalan Bailey (Pirbright Institute, Pirbright, United Kingdom) for providing plasmid templates to allow for the generation of reagents for the bimolecular complementation assay; the Animal Science Core team at National Emerging Infectious Diseases Laboratory (NEIDL), Boston University for excellent animal study support; Rik de Swart and Rory de Vries (Erasmus Medical Center, Rotterdam, the Netherlands) for advice regarding animal sample collection, sample processing, and assay development; and Christopher Richardson (Dalhousie University, Halifax, NS, Canada) for constructive comments and the provision of nectin-4–expressing cells used for the experiments we conducted during revision. We appreciate the foresight of Scott Brown and Zach Mills (Zoetis External Innovation and Research Alliances) in believing in this program from an early stage in its inception. This work was supported by Zoetis LLC and The University of Pittsburgh and utilized a Vectra Polaris whole-slide scanner purchased with an NIH Shared Instrument Grant S10OD030269 (to N.A.C.).

Author affiliations: [a]Center for Vaccine Research, University of Pittsburgh School of Medicine, Pittsburgh, PA 15261; [b]Department of Microbiology and Molecular Genetics, University of Pittsburgh School of Medicine, Pittsburgh, PA 15261; [c]National Emerging Infectious Diseases Laboratories, Boston University, Boston, MA 02118; [d]Department of Pathology and Laboratory Medicine, Boston University School of Medicine, Boston, MA 02118; [e]Veterinary Medicine Research & Development, Zoetis LLC, Kalamazoo, MI 49007; [f]School of Veterinary Medicine, Murdoch University, Murdoch, WA 6150, Australia; and [g]Department of Clinical Sciences,Tufts Cummings School of Veterinary Medicine, North Grafton, MA 01536

1. P. C. Woo *et al.*, Feline morbillivirus, a previously undescribed paramyxovirus associated with tubulointerstitial nephritis in domestic cats. *Proc. Natl. Acad. Sci. U.S.A.* **109**, 5435–5440 (2012).
2. D. Kolakofsky *et al.*, Paramyxovirus RNA synthesis and the requirement for hexamer genome length: The rule of six revisited. *J. Virol.* **72**, 891–899 (1998).
3. S. Nambulli, C. R. Sharp, A. S. Acciardo, J. F. Drexler, W. P. Duprex, Mapping the evolutionary trajectories of morbilliviruses: What, where and whither. *Curr. Opin. Virol.* **16**, 95–105 (2016).
4. B. Rima *et al.*, Problems of classification in the family Paramyxoviridae. *Arch. Virol.* **163**, 1395–1404 (2018).
5. A. Zeltina, T. A. Bowden, B. Lee, Emerging paramyxoviruses: Receptor tropism and zoonotic potential. *PLoS Pathog.* **12**, e1005390 (2016).
6. H. Tatsuo, N. Ono, K. Tanaka, Y. Yanagi, SLAM (CDw150) is a cellular receptor for measles virus. *Nature* **406**, 893–897 (2000).
7. R. E. Dutch, T. S. Jardetzky, R. A. Lamb, Virus membrane fusion proteins: Biological machines that undergo a metamorphosis. *Biosci. Rep.* **20**, 597–612 (2000).
8. H. Yilmaz *et al.*, Frequency, clinicopathological features and phylogenetic analysis of feline morbillivirus in cats in Istanbul, Turkey. *J. Feline Med. Surg.* **19**, 1206–1214 (2017).
9. N. H. Mohd Isa *et al.*, Molecular detection and characterisation of feline morbillivirus in domestic cats in Malaysia. *Vet. Microbiol.* **236**, 108382 (2019).
10. T. Furuya *et al.*, Existence of feline morbillivirus infection in Japanese cat populations. *Arch. Virol.* **159**, 371–373 (2014).
11. S. Sakaguchi *et al.*, Genetic diversity of feline morbilliviruses isolated in Japan. *J. Gen. Virol.* **95**, 1464–1468 (2014).
12. J. Ou *et al.*, First report of feline morbillivirus in mainland China. *Arch. Virol.* **165**, 1837–1841 (2020).
13. S. Chaiyasak, C. Piewbang, A. Rungsipipat, S. Techangamsuwan, Molecular epidemiology and genome analysis of feline morbillivirus in household and shelter cats in Thailand. *BMC Vet. Res.* **16**, 240 (2020).
14. K. E. McCallum *et al.*, Detection and seroprevalence of morbillivirus and other paramyxoviruses in geriatric cats with and without evidence of azotemic chronic kidney disease. *J. Vet. Intern. Med.* **32**, 1100–1108 (2018).
15. A. Lorusso *et al.*, First report of feline morbillivirus in Europe. *Vet. Ital.* **51**, 235–237 (2015).
16. M. Sieg *et al.*, Discovery of new feline paramyxoviruses in domestic cats with chronic kidney disease. *Virus Genes* **51**, 294–297 (2015).
17. C. R. Sharp *et al.*, Chronic infection of domestic cats with feline morbillivirus, United States. *Emerg. Infect. Dis.* **22**, 760–762 (2016).
18. G. M. Darold *et al.*, First report of feline morbillivirus in South America. *Arch. Virol.* **162**, 469–475 (2017).
19. J. Busch *et al.*, High seroprevalence of feline morbilliviruses in free-roaming domestic cats in Chile. *Arch. Virol.* **166**, 281–285 (2021).
20. P. E. Crisi *et al.*, Early renal involvement in cats with natural feline morbillivirus infection. *Animals (Basel)* **10**, 828 (2020).
21. A. Stranieri *et al.*, Feline morbillivirus in Northern Italy: Prevalence in urine and kidneys with and without renal disease. *Vet. Microbiol.* **233**, 133–139 (2019).
22. O. A. Negrete *et al.*, EphrinB2 is the entry receptor for Nipah virus, an emergent deadly paramyxovirus. *Nature* **436**, 401–405 (2005).
23. M. I. Bonaparte *et al.*, Ephrin-B2 ligand is a functional receptor for Hendra virus and Nipah virus. *Proc. Natl. Acad. Sci. U.S.A.* **102**, 10652–10657 (2005).
24. M. Bieringer *et al.*, Experimental adaptation of wild-type canine distemper virus (CDV) to the human entry receptor CD150. *PLoS One* **8**, e57488 (2013).
25. C. T. Pager, W. W. Craft Jr., J. Patch, R. E. Dutch, A mature and fusogenic form of the Nipah virus fusion protein requires proteolytic processing by cathepsin L. *Virology* **346**, 251–257 (2006).
26. C. T. Pager, R. E. Dutch, Cathepsin L is involved in proteolytic processing of the Hendra virus fusion protein. *J. Virol.* **79**, 12714–12720 (2005).
27. S. Diederich *et al.*, Activation of the Nipah virus fusion protein in MDCK cells is mediated by cathepsin B within the endosome-recycling compartment. *J. Virol.* **86**, 3736–3745 (2012).
28. T. Hashiguchi *et al.*, Structure of the measles virus hemagglutinin bound to its cellular receptor SLAM. *Nat. Struct. Mol. Biol.* **18**, 135–141 (2011).
29. M. Mateo, C. K. Navaratnarajah, S. Syed, R. Cattaneo, The measles virus hemagglutinin β-propeller head β4-β5 hydrophobic groove governs functional interactions with nectin-4 and CD46 but not those with the signaling lymphocytic activation molecule. *J. Virol.* **87**, 9208–9216 (2013).
30. N. Massé *et al.*, Measles virus (MV) hemagglutinin: Evidence that attachment sites for MV receptors SLAM and CD46 overlap on the globular head. *J. Virol.* **78**, 9051–9063 (2004).
31. S. Vongpunsawad, N. Oezgun, W. Braun, R. Cattaneo, Selectively receptor-blind measles viruses: Identification of residues necessary for SLAM- or CD46-induced fusion and their localization on a new hemagglutinin structural model. *J. Virol.* **78**, 302–313 (2004).
32. L. Zipperle *et al.*, Identification of key residues in virulent canine distemper virus hemagglutinin that control CD150/SLAM-binding activity. *J. Virol.* **84**, 9618–9624 (2010).
33. V. von Messling *et al.*, Nearby clusters of hemagglutinin residues sustain SLAM-dependent canine distemper virus entry in peripheral blood mononuclear cells. *J. Virol.* **79**, 5857–5862 (2005).
34. F. Xu *et al.*, Computational analysis of the interaction energies between amino acid residues of the measles virus hemagglutinin and its receptors. *Viruses* **10**, 236 (2018).
35. M. Sieg *et al.*, A new genotype of feline morbillivirus infects primary cells of the lung, kidney, brain and peripheral blood. *Viruses* **11**, 146 (2019).
36. M. Sieg, A. Vahlenkamp, C. G. Baums, T. W. Vahlenkamp, First complete genome sequence of a feline morbillivirus isolate from Germany. *Genome Announc.* **6**, e00244-18 (2018).
37. J. Y. Xin, T. Ihara, K. Komase, T. Nakayama, Amino acid substitutions in matrix, fusion and hemagglutinin proteins of wild measles virus for adaptation to vero cells. *Intervirology* **54**, 217–228 (2011).
38. D. W. Kouomou, T. F. Wild, Adaptation of wild-type measles virus to tissue culture. *J. Virol.* **76**, 1505–1509 (2002).
39. B. K. Rima *et al.*, Sequence divergence of measles virus haemagglutinin during natural evolution and adaptation to cell culture. *J. Gen. Virol.* **78**, 97–106 (1997).
40. D. Naniche *et al.*, Human membrane cofactor protein (CD46) acts as a cellular receptor for measles virus. *J. Virol.* **67**, 6025–6032 (1993).
41. R. E. Dörig, A. Marcil, A. Chopra, C. D. Richardson, The human CD46 molecule is a receptor for measles virus (Edmonston strain). *Cell* **75**, 295–305 (1993).
42. M. Watanabe *et al.*, Engineered serine protease inhibitor prevents furin-catalyzed activation of the fusion glycoprotein and production of infectious measles virus. *J. Virol.* **69**, 3206–3210 (1995).
43. H. C. Aguilar, B. A. Henderson, J. L. Zamora, G. P. Johnston, Paramyxovirus glycoproteins and the membrane fusion process. *Curr. Clin. Microbiol. Rep.* **3**, 142–154 (2016).
44. R. Koide, S. Sakaguchi, T. Miyazawa, Basic biological characterization of feline morbillivirus. *J. Vet. Med. Sci.* **77**, 565–569 (2015).
45. M. Montaser, G. Lalmanach, L. Mach, CA-074, but not its methyl ester CA-074Me, is a selective inhibitor of cathepsin B within living cells. *Biol. Chem.* **383**, 1305–1308 (2002).
46. K. Chandran, N. J. Sullivan, U. Felbor, S. P. Whelan, J. M. Cunningham, Endosomal proteolysis of the Ebola virus glycoprotein is necessary for infection. *Science* **308**, 1643–1645 (2005).
47. J. K. Millet, G. R. Whittaker, Host cell proteases: Critical determinants of coronavirus tropism and pathogenesis. *Virus Res.* **202**, 120–134 (2015).
48. V. von Messling, D. Milosevic, R. Cattaneo, Tropism illuminated: Lymphocyte-based pathways blazed by lethal morbillivirus through the host immune system. *Proc. Natl. Acad. Sci. U.S.A.* **101**, 14216–14221 (2004).
49. R. L. de Swart *et al.*, Predominant infection of CD150+ lymphocytes and dendritic cells during measles virus infection of macaques. *PLoS Pathog.* **3**, e178 (2007).

50. M. Ludlow *et al.*, Recombinant canine distemper virus strain Snyder Hill expressing green or red fluorescent proteins causes meningoencephalitis in the ferret. *J. Virol.* **86**, 7508–7519 (2012).
51. K. Lemon *et al.*, Recombinant subgroup B human respiratory syncytial virus expressing enhanced green fluorescent protein efficiently replicates in primary human cells and is virulent in cotton rats. *J. Virol.* **89**, 2849–2856 (2015).
52. K. Lemon *et al.*, Early target cells of measles virus after aerosol infection of non-human primates. *PLoS Pathog.* **7**, e1001263 (2011).
53. R. D. de Vries *et al.*, Delineating morbillivirus entry, dissemination and airborne transmission by studying in vivo competition of multicolor canine distemper viruses in ferrets. *PLoS Pathog.* **13**, e1006371 (2017).
54. H. S. El Mubarak *et al.*, Infection of cynomolgus macaques (Macaca fascicularis) and rhesus macaques (Macaca mulatta) with different wild-type measles viruses. *J. Gen. Virol.* **88**, 2028–2034 (2007).
55. H. M. Coovadia *et al.*, Alterations in immune responsiveness in acute measles and chronic post-measles chest disease. *Int. Arch. Allergy Appl. Immunol.* **56**, 14–23 (1978).
56. B. McCullough, S. Krakowka, A. Koestner, Experimental canine distemper virus-induced lymphoid depletion. *Am. J. Pathol.* **74**, 155–170 (1974).
57. R. D. de Vries *et al.*, Measles immune suppression: Lessons from the macaque model. *PLoS Pathog.* **8**, e1002885 (2012).
58. R. D. de Vries *et al.*, In vivo tropism of attenuated and pathogenic measles virus expressing green fluorescent protein in macaques. *J. Virol.* **84**, 4714–4724 (2010).
59. L. M. Esolen, B. J. Ward, T. R. Moench, D. E. Griffin, Infection of monocytes during measles. *J. Infect. Dis.* **168**, 47–52 (1993).
60. M. Ludlow *et al.*, Infection of lymphoid tissues in the macaque upper respiratory tract contributes to the emergence of transmissible measles virus. *J. Gen. Virol.* **94**, 1933–1944 (2013).
61. S. Chaiyasak *et al.*, Renal epitheliotropism of feline morbillivirus in two cats. *Vet. Pathol.* **59**, 127–131 (2022).
62. T. Ihara *et al.*, Markedly elevated levels of beta2-microglobulin in urine with measles viruria in patients with measles. *Clin. Diagn. Virol.* **4**, 285–291 (1995).
63. G. Elia *et al.*, Detection of canine distemper virus in dogs by real-time RT-PCR. *J. Virol. Methods* **136**, 171–176 (2006).
64. D. T. Shen, J. R. Gorham, V. Pedersen, Viruria in dogs infected with canine distemper. *Vet. Med. Small Anim. Clin.* **76**, 1175–1177 (1981).
65. E. S. Park *et al.*, Epidemiological and pathological study of feline morbillivirus infection in domestic cats in Japan. *BMC Vet. Res.* **12**, 228 (2016).
66. M. D. Mühlebach *et al.*, Adherens junction protein nectin-4 is the epithelial receptor for measles virus. *Nature* **480**, 530–533 (2011).
67. R. S. Noyce *et al.*, Tumor cell marker PVRL4 (nectin 4) is an epithelial cell receptor for measles virus. *PLoS Pathog.* **7**, e1002240 (2011).
68. X. Zhang *et al.*, Structure of measles virus hemagglutinin bound to its epithelial receptor nectin-4. *Nat. Struct. Mol. Biol.* **20**, 67–72 (2012).
69. S. Delpeut, R. S. Noyce, C. D. Richardson, The tumor-associated marker, PVRL4 (nectin-4), is the epithelial receptor for morbilliviruses. *Viruses* **6**, 2268–2286 (2014).
70. L. T. Lin, C. D. Richardson, The host cell receptors for measles virus and their interaction with the viral hemagglutinin (H) protein. *Viruses* **8**, 250 (2016).
71. M. Mateo *et al.*, Different roles of the three loops forming the adhesive interface of nectin-4 in measles virus binding and cell entry, nectin-4 homodimerization, and heterodimerization with nectin-1. *J. Virol.* **88**, 14161–14171 (2014).
72. T. Cathomen, C. J. Buchholz, P. Spielhofer, R. Cattaneo, Preferential initiation at the second AUG of the measles virus F mRNA: A role for the long untranslated region. *Virology* **214**, 628–632 (1995).
73. N. L. Tilston-Lunel *et al.*, Sustained replication of synthetic canine distemper virus defective genomes *in vitro* and *in vivo*. *MSphere* **6**, e0053721 (2021).
74. B. H. Harcourt *et al.*, Molecular characterization of Nipah virus, a newly emergent paramyxovirus. *Virology* **271**, 334–349 (2000).
75. J. T. Kelly *et al.*, BST2/Tetherin overexpression modulates morbillivirus glycoprotein production to inhibit cell-cell fusion. *Viruses* **11**, 692 (2019).
76. H. Ishikawa, F. Meng, N. Kondo, A. Iwamoto, Z. Matsuda, Generation of a dual-functional split-reporter protein for monitoring membrane fusion using self-associating split GFP. *Protein Eng. Des. Sel.* **25**, 813–820 (2012).
77. M. S. Sidhu *et al.*, Rescue of synthetic measles virus minireplicons: Measles genomic termini direct efficient expression and propagation of a reporter gene. *Virology* **208**, 800–807 (1995).
78. N. Thakur *et al.*, Micro-fusion inhibition tests: Quantifying antibody neutralization of virus-mediated cell-cell fusion. *J. Gen. Virol.* **102**, jgv001506 (2021).
79. L. J. Rennick *et al.*, Recombinant subtype A and B human respiratory syncytial virus clinical isolates co-infect the respiratory tract of cotton rats. *J. Gen. Virol.* **101**, 1056–1068 (2020).
80. K. Lemon, B. K. Rima, S. McQuaid, I. V. Allen, W. P. Duprex, The F gene of rodent brain-adapted mumps virus is a major determinant of neurovirulence. *J. Virol.* **81**, 8293–8302 (2007).
81. L. J. Reed, H. Muench, A simple method for estimating fifty percent endpoints. *Am. J. Hyg.* **27**, 493–497 (1938).
82. C. E. Stewart, R. E. Randall, C. S. Adamson, Inhibitors of the interferon response enhance virus replication in vitro. *PLoS One* **9**, e112014 (2014).